Melting in Large Sodium Clusters: An Orbital-Free Molecular Dynamics Study

Andrés Aguado,* Jose M. López, and Julio A. Alonso

Departamento de Física Teórica, Universidad de Valladolid, Valladolid 47011, Spain

M. J. Stott

Department of Physics, Queen's University, Kingston, Ontario K7L 3N6, Canada

Received: May 18, 2000; In Final Form: December 6, 2000

The melting-like transition in sodium clusters Na_N, with $N = 55$, 92, and 142, is studied by using constant-energy molecular dynamics simulations. An orbital-free version of the Car−Parrinello technique is used that scales linearly with system size, allowing for investigations of the thermal behavior of large clusters. The ground-state isomer of Na_{142} (an incomplete three-shell icosahedron) melts in two steps: the first (at ∼240 K) is characterized by the high mobility of atoms located on the cluster surface, and the second, homogeneous melting (at ∼270 K) involves diffusive motion of all of the atoms across the cluster. For the case of Na_{92}, the icosahedral structure has a larger number of surface vacancies and melts in two well-separated steps, with surface melting at ∼130 K and homogeneous melting at ∼240 K. Na_{55}, a complete two-shell icosahedron, melts in a single stage at ∼190 K. Our results on homogeneous melting for Na_{142} and Na_{92} are in excellent agreement with recent experimental determinations of melting temperatures and latent heats. However, the experimentally observed enhancement of the melting temperature around $N = 55$ is not reproduced by the calculations.

I. Introduction

The melting-like transition in finite clusters consisting of a small number of atoms is of fundamental interest, as clusters are often produced in a disordered "liquid" state,[1] and it is also relevant to applications of clusters. For example, the catalytic activity of small platinum clusters depends critically on their melting temperatures.[2] Recent experimental advances reveal some details of the melting-like transition but, at the same time, show new and interesting features. Martin[3] determined the cluster-size dependence of the melting temperature T_m of large sodium clusters, composed of thousands of atoms, by observing the vanishing of the atomic-shell structure in the mass spectra upon heating. It was concluded that T_m grows with cluster size, but the results did not yet extrapolate to the T_m of the bulk. Peters et al.[4] performed X-ray diffraction experiments on large (50-nm) Pb clusters and observed the occurrence of surface melting before homogeneous melting. Electron diffraction[5] might also help in detecting a surface melting stage.[2] Haberland and co-workers[6] studied the variation with temperature of the photofragmentation spectra of Na_N ($N = 50-200$) clusters and deduced the melting temperatures of the clusters. They find that, for some cluster sizes, the melting temperature is a local maximum not in exact correspondence with either electronic- or atomic-shell closing numbers, but bracketed by the two, suggesting that both effects are relevant to the melting process.

A number of computer simulations of melting in small metallic and nonmetallic clusters have been reported, the majority of which employed phenomenological interatomic potentials.[7−10] The use of such parametrized potentials allows for the consideration of long dynamical trajectories for large clusters.[8,9] Ab initio methods,[11] which have also been used, accurately treat the electronic structure of the cluster but are much more expensive computationally and are usually restricted to the study of small clusters for short dynamical trajectories.[12] Recently, Rytkönen et al.[13] performed ab initio molecular dynamics (aiMD) simulations of the melting of a sodium cluster with 40 atoms, but such a large cluster required the use of a fast heating rate. These aiMD treatments use the Kohn−Sham (KS) form[14] of density functional theory (DFT), and orthogonalization of the one-electron KS orbitals is the limiting step in their performance. However, DFT shows that the total energy of the electronic system can be expressed in terms of just the electronic density,[15] and orbital-free (OF) versions of the aiMD technique based on the electron density have been developed and employed, both for solid-state[16−18] and cluster[19−22] applications. These OF methods scale linearly with the system size, allowing for the study of larger clusters for longer simulation times than typical aiMD simulations. However, quantum-shell effects are neglected, so that features associated with electronic-shell closings are not reproduced.

Previously,[22] we used the orbital-free molecular dynamics (OFMD) method to study the melting process in small sodium clusters, Na_8 and Na_{20}, clusters outside the range covered by Haberland's photofragmentation experiments.[6] Here, we report constant-energy OFMD simulations in a study of the melting-like transition in larger clusters, namely Na_{55}, Na_{92}, and Na_{142}, which are within the size range covered in those experiments and for which a full ab initio treatment of their thermal properties would be impractical. Even for the OFMD method, these large clusters represent a substantial computational effort. The aim of our work is to study the mechanisms by which the melting-like transition proceeds in these large clusters. In the next section, we briefly present some technical details of the method. The results are presented and discussed in section III, and finally, section IV summarizes our main conclusions.

* Author to whom correspondence should be addressed. Present address: Physical and Theoretical Chemistry Laboratory, University of Oxford, South Parks Road, Oxford OX1 3QZ, UK.

10.1021/jp0018504 CCC: $20.00
Published on Web 03/01/2001

II. Theory

The orbital-free molecular dynamics method is a Car−Parrinello total energy scheme[11] that uses an explicit kinetic-energy functional of the electron density and the electron density as the dynamical variable, as opposed to the KS single-particle wave functions. In contrast to simulations that use empirical interatomic potentials, the detailed electronic structure and the electronic contributions to the energy and the forces on the ions are recalculated efficiently at every atomic time step. The main features of the energy functional and the calculational scheme have been described at length in previous works,[17,19,21,22] and details of our method are as described in Aguado et al.[22] In brief, the electronic kinetic energy functional of the electron density, $n(\vec{r})$, corresponds to the gradient expansion around the homogeneous limit through second order[15,23−25]

$$T_s[n] = T^{TF}[n] + \frac{1}{9}T^{W}[n] \tag{1}$$

where the first term is the Thomas−Fermi functional

$$T^{TF}[n] = \frac{3}{10}(3\pi^2)^{2/3}\int n(\vec{r})^{5/3}\,d\vec{r} \tag{2}$$

and the second is the lowest-order gradient correction, with T^W, the von Weizsäcker term, given by

$$T^{W}[n] = \frac{1}{8}\int \frac{|\nabla n(\vec{r})|^2}{n(\vec{r})}\,d\vec{r} \tag{3}$$

The local density approximation is used for exchange and correlation.[26,27] In the external field acting on the electrons, $V_{ext}(\vec{r}) = \sum_n v(\vec{r} - \vec{R}_n)$, we take v to be the local pseudopotential of Fiolhais et al.,[28] which reproduces well the properties of bulk sodium and which has been shown to have good transferability to sodium clusters.[29]

The cluster is placed in a unit cell of a cubic superlattice, and the set of plane waves periodic in the superlattice is used as a basis set for expansion of the valence density. Following Car and Parrinello,[11] the coefficients of that expansion are regarded as generalized coordinates of a set of fictitious classical particles, and the corresponding Lagrange equations of motion for the ions and the electron density distribution are solved as described in ref 22.

The calculations for Na_{92} and Na_{142} used a supercell of edge 71 au and an energy cutoff in the plane-wave expansion of the density of 8 Ry. For Na_{55}, the cell edge was 64 au, and the energy cutoff was 10 Ry. In all cases, a $64 \times 64 \times 64$ grid was used. Previous tests[22] indicate that the cutoffs used give good convergence of bond lengths and binding energies. The fictitious mass associated with the electron density coefficients ranged between 1.0×10^8 and 3.3×10^8 au, and the equations of motion were integrated using the Verlet algorithm[30] for both electrons and ions with a time step ranging from $\Delta t = 0.73 \times 10^{-15}$ s for the simulations performed at the lowest temperatures, to $\Delta t = 0.34 \times 10^{-15}$ s for those at the highest temperatures. These choices resulted in a conservation of the total energy to better than 0.1%.

The first step of the simulations was the determination of the low-temperature isomers for each of the three cluster sizes. For such large clusters, it is very difficult to find the global minimum because the number of different local minima increases exponentially with the number of atoms in the cluster. Instead, one has to adopt structures that are likely to have the main characteristics of the ground state. We assumed icosahedral growth. Thus, for Na_{142}, we removed five atoms from the surface of a 147-atom three-shell perfect icosahedron. For Na_{92}, we constructed an icosahedral isomer by following the growth sequence described by Montejano-Carrizales et al.,[31] and for Na_{55}, we took a perfect two-shell icosahedron. We also used dynamical simulated annealing[11] to generate low-temperature isomers, but this procedure always led to amorphous structures for Na_{92} and Na_{142} (less stable than the icosahedral ones) and to a nearly icosahedral structure for Na_{55}.

Several molecular dynamics simulation runs at different constant energies were performed in order to obtain the caloric curve for each icosahedral isomer. The initial positions of the atoms for the first run were determined by slightly deforming the equilibrium low-temperature geometry of the isomer. The final configuration of each run served as the starting geometry for the next run at a different energy. The initial velocities for every new run were obtained by scaling the final velocities of the preceding run. The total simulation time was 20 ps for each run at constant energy.

A number of indicators for locating the melting-like transition were employed. Namely, these are the specific heat per particle (in units of the Boltzman constant), defined by[32]

$$C_v = \left[N - N\left(1 - \frac{2}{3N-6}\right)\langle E_{kin}\rangle_t\langle E_{kin}{}^{-1}\rangle_t\right]^{-1} \tag{4}$$

where N is the number of atoms and $\langle\ \rangle_t$ indicates the average along a trajectory; the diffusion coefficient

$$D = \frac{1}{6}\frac{d}{dt}\langle r^2(t)\rangle \tag{5}$$

which is obtained from the long-time behavior of the mean square displacement

$$\langle r^2(t)\rangle = \frac{1}{Nn_t}\sum_{j=1}^{n_t}\sum_{i=1}^{N}[\vec{R}_i(t_{0_j}+t) - \vec{R}_i(t_{0_j})]^2$$

where n_t is the number of time origins, t_{0_j}, considered along a trajectory; the time evolution of the distance between each atom and the center of mass of the cluster

$$r_i(t) = |\vec{R}_i(t) - \vec{R}_{cm}(t)| \tag{6}$$

and finally, the radial atomic density, averaged over an entire dynamical trajectory

$$\rho(r) = \frac{dN_{at}(r)/dr}{4\pi r^2} \tag{7}$$

where $dN_{at}(r)$ is the number of atoms at distances from the center of mass between r and $r + dr$.

In the next section, we present the results for several of these quantities in terms of the internal cluster temperature, which we define through the equipartition expression[32]

$$T = \frac{2\langle E_k\rangle}{3N-6} \tag{8}$$

where we have taken into account the fact that the position of the center of mass of the cluster was fixed and the total momentum was held to zero during the simulations, reducing from $3N$ to $(3N - 6)$ the number of degrees of freedom of the system. With this choice for the temperature, the correct low-temperature asymptotic limit of the specific heat per particle, namely, $3k_B$, is reproduced. Our expression for C_v corresponds

to that given by Pearson et al.[33] (with the only change being in the number of degrees of freedom, for consistency with the temperature), so that it also reproduces the correct $N \rightarrow \infty$ asymptotic limit.

III. Results

The lowest-energy structure of sodium clusters of medium size is not known. DFT calculations for Na_{55} performed by Kummel et al.[34] using an approximate structural model (CAPS model, in which the total pseudopotential of the ionic skeleton is cylindrically averaged)[35] give a structure close to icosahedral. Near-threshold photoionization mass spectrometry experiments suggest icosahedral structures for large sodium clusters with more than 1400 atoms,[36] so incomplete icosahedral structures are plausible candidates for Na_{92} and Na_{142}. For this reason we adopted for Na_{142} an isomer obtained by removing five atoms from a perfect three-shell icosahedron. The icosahedral growth sequence in nickel clusters has been studied by Montejano-Carrizales et al.,[31] who showed that the 12 vertices of the outermost shell are the last sites to be occupied. Assuming the same growth sequence for sodium clusters, we removed five atoms from the vertex positions of Na_{147}, testing all possibilities, and then relaxed the resulting structures. In the most stable structure thus formed, the five vacancies form a pentagon. For Na_{92}, we adopted the umbrella growth model of Montejano-Carrizales et al.[31] The resulting structure corresponds to three complete umbrellas capping a Na_{55} icosahedron. Low-temperature dynamical trajectories verify that these structures are indeed stable isomers of Na_{92} and Na_{142}. The icosahedral isomers are more stable than the lowest-energy amorphous isomers which were found by simulated annealing (0.017 and 0.020 eV/atom more stable for Na_{92} and Na_{142}, respectively). Calvo and Spiegelmann studied sodium clusters in the same size range, using pair potential and tight-binding (TB) calculations,[9] and also predicted icosahedral structures for Na_{55},Na_{93}, Na_{139}, and Na_{147}.

For each icosahedral cluster, we calculated the so-called caloric curve, which is the internal temperature as a function of the total energy. A thermal phase transition is indicated in the caloric curve by a change in slope, the slope being the specific heat; the height of the step gives an estimate of the latent heat of fusion. However, melting processes are more easily recognized as peaks in the specific heat as a function of temperature. These peaks have been calculated directly from eq 4 and are shown, together with the caloric curves, in Figures 1−3. The specific heat peaks occur at the same temperatures as the slope changes of the caloric curve, giving us confidence in the convergence of our results as the two quantities were obtained in different ways.

The specific heat curve for Na_{142} (Figure 1) displays two main peaks at $T_s \approx 240$ K and $T_m \approx 270$ K, suggesting a two-step melting process. The two peaks are so close, however, that only one slope change in the caloric curve can be distinguished. Our analysis below shows that homogeneous melting occurs at $T_m \approx 270$ K, in excellent agreement with the experiments of Haberland and co-workers,[6] who give an approximate value of 280 K. The latent heat of fusion estimated from the step at T_m in the caloric curve is $q_m \approx 15$ meV/atom, again in good agreement with the experimental value of 14 meV/atom. The premelting stage at $T = T_s$ is not detected in the experiments, but our results are not inconsistent with experiment because the two calculated peaks in the specific heat are close together and the height of the first peak is much smaller than that of the second; consequently, they would be difficult to distinguish experimentally. Calvo and Spiegelmann[9] have performed Monte

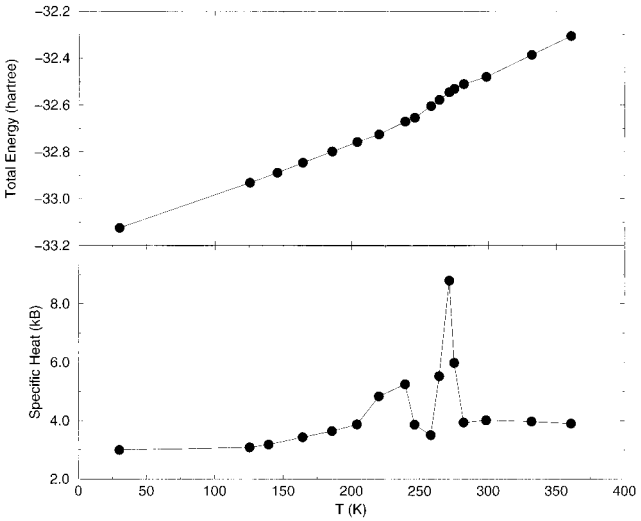

Figure 1. Caloric and specific heat curves of Na_{142}, taking the internal cluster temperature as the independent variable. The deviation around the mean temperature is smaller than the size of the circles.

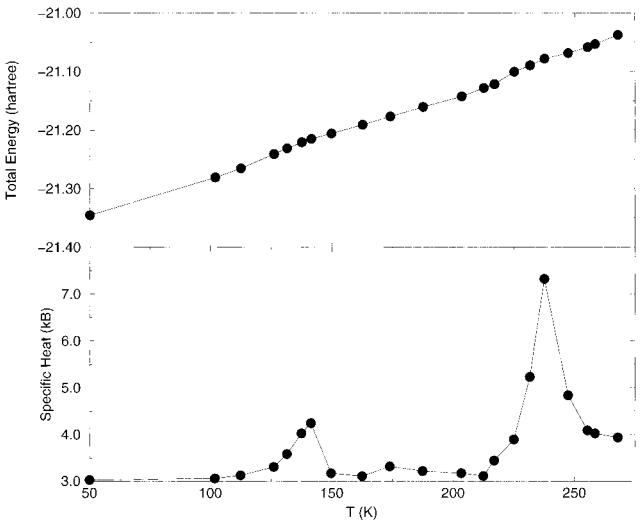

Figure 2. Caloric and specific heat curves of Na_{92}, taking the internal cluster temperature as the independent variable. The deviation around the mean temperature is smaller than the size of the circles.

Carlo (MC) simulations using a semiempirical many-atom potential, and the lowest-energy isomer they found for Na_{139} was also an incomplete three-shell icosahedron, in this case with eight surface vacancies. They also report two close peaks in the specific heat curve, indicating a two-step melting process with $T_s \approx 210$ K and $T_m \approx 230$ K. They concluded that these two temperatures become closer as the cluster size increases, so that, for clusters with more than about 100 atoms, there is effectively just one peak in the specific heat and a single-step melting. Tight-binding (TB) molecular dynamics calculations were performed by the same authors.[9] Although the melting temperatures were found to be different from those obtained with the semiempirical potentials (TB tends to overestimate the experimental values, while empirical potentials tend to underestimate them), the qualitative picture of melting in two close steps was the same.

The results for Na_{92} are shown in Figure 2. Two-step melting is again observed, with a small prepeak in the specific heat at $T_s \approx 130$ K and a large peak corresponding to homogeneous melting at $T_m \approx 240$ K. In this case, T_s and T_m are well-separated, but the first peak is much smaller than the second, which could again account for the absence of the prepeak in

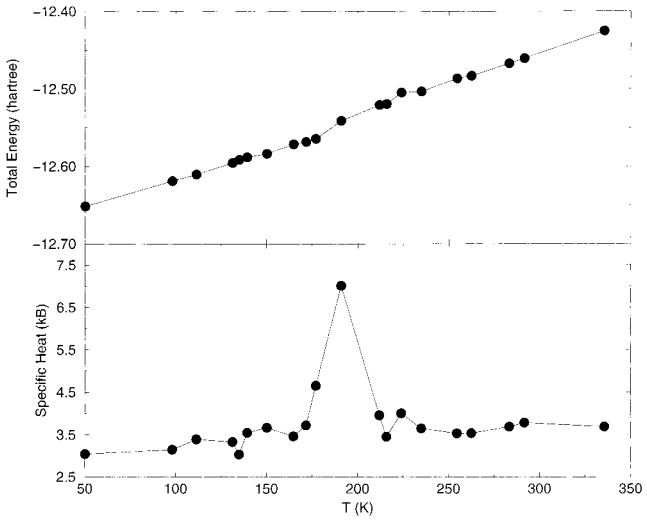

Figure 3. Caloric and specific heat curves of Na_{55}, taking the internal cluster temperature as the independent variable. The deviation around the mean temperature is smaller than the size of the circles.

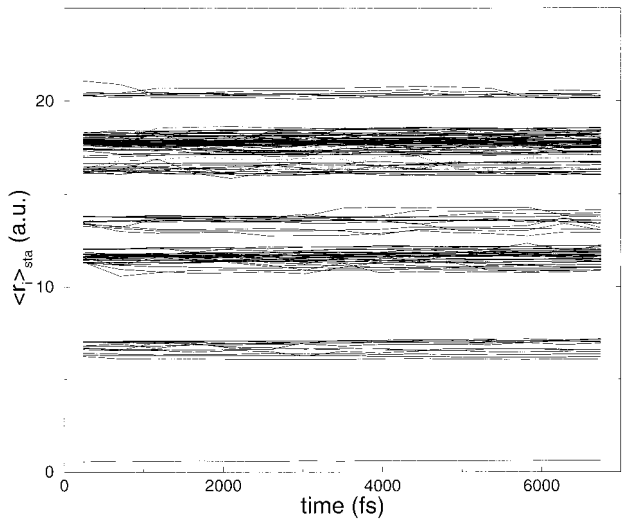

Figure 4. Short-time-averaged distances $\langle r_i(t)\rangle_{sta}$ between each atom and the center of mass in Na_{142}, as functions of time for the icosahedral isomer at $T = 30$ K.

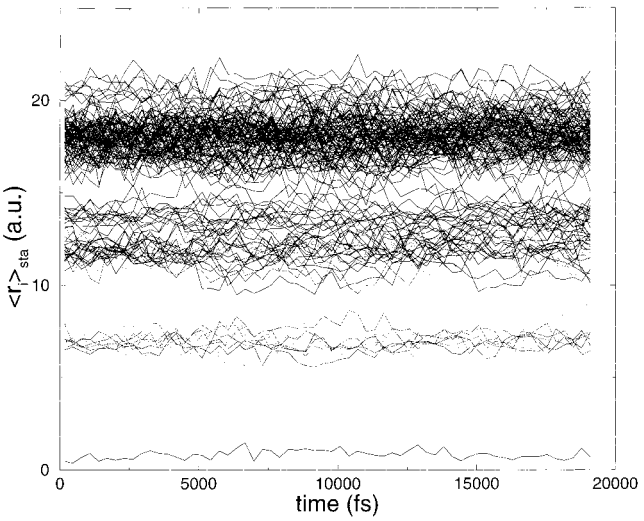

Figure 5. Short-time-averaged distances $\langle r_i(t)\rangle_{sta}$ between each atom and the center of mass in Na_{142}, as functions of time for the icosahedral isomer at $T = 160$ K.

the experiments. The calculated temperature and latent heat for the homogeneous melting stage, $T_m \approx 240$ K and $q_m \approx 8$ meV/atom, are again in excellent agreement with the experimental values,[6] 250 K and 7 meV/atom, respectively. Calvo and Spiegelmann[9] arrive at similar conclusions based on MC simulations for Na_{93} using phenomenological potentials: a small bump near 100 K and a main peak near 180 K. Their TB simulations give values for those two temperatures that are roughly 100 K higher.

The experiments[6] indicate a substantial enhancement of the melting temperature in the size region around $N = 55$ atoms. The reported melting temperature of Na_{55}^+ is 325 K, surprisingly higher than that of Na_{142}^+, which is a local maximum in the size region of the third icosahedral-shell closing. Our simulations do not reproduce this enhancement of T_m for Na_{55} and predict that this cluster melts in a single stage at $T_m \approx 190$ K (Figure 3), a result found also by Calvo and Spiegelmann.[9] Our implementation of the OFMD method, which employs a semilocal electronic kinetic energy operator, does not account for electronic quantum-shell effects. Consequently, OFMD simulations with fully nonlocal $T_s[n]$ operators[16−18] or orbital-based KS calculations might be needed to clarify this discrepancy, although it is not clear a priori how electronic-shell effects could shift the value of T_m by such a large amount. Of course, another possibility is that the icosahedron is not the ground-state isomer. However, Kümmel et al.[34] have recently found that the experimental photoabsorption spectrum of Na_{55}^+ is best reproduced with a slightly oblate isomer that is close to icosahedral. We have also investigated a bcc-like growth sequence, finding that bcc structures are less stable than icosahedral ones for all cluster sizes studied. Also, we studied the melting behavior of a Na_{55} isomer with a bcc structure and did not find an enhanced melting temperature for it either. In summary, the discrepancy between experiment and theory for Na_{55} requires further attention.

Various quantities were analyzed in order to investigate the nature of the transitions at T_s and T_m. The short-time averages (sta) of the distances between each atom and the center of mass of the cluster, $\langle r_i(t)\rangle_{sta}$, were calculated, and the cluster evolution during the trajectories was followed visually using computer graphics. The $\langle r_i(t)\rangle_{sta}$ curves for Na_{142} are presented in Figures 4−6 for three representative temperatures. At low temperatures (Figure 4), the values of $\langle r_i(t)\rangle_{sta}$ are almost independent of time. The movies show that the clusters are solid, with the atoms merely vibrating around their equilibrium positions. Curve crossings are due to oscillatory motion and slight structural relaxations rather than diffusive motion. At this low temperature, quasidegenerate groups that are characteristic of the symmetry can be distinguished: One line near the center of mass of the cluster identifies the central atom (its position does not exactly coincide with the center of mass because of the location of the five surface vacancies). Twelve lines correspond to the first icosahedral shell. Another 42 lines complete the second shell, within which we can distinguish the 12 vertex atoms from the rest because their distances to the center of mass are slightly larger. Finally, 82 lines describe the external shell, where again we can distinguish the 7 vertex atoms from the rest.

The radial atomic density distributions with respect to the cluster center, $\rho(r)$, are shown for Na_{142} in Figure 7. At the lowest temperature, $T = 30$ K, the atoms in the icosohedral isomer are distributed in three well-separated shells, a surface shell and two inner shells. As discussed above, subshells form in the second and third shells. The shell structure is still present at $T = 130$ K.

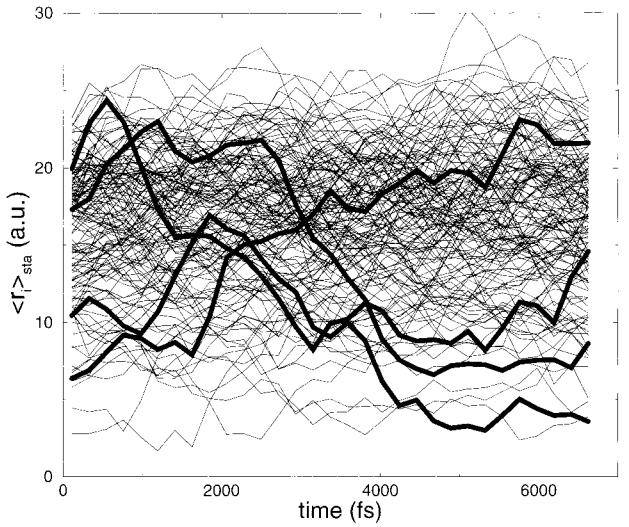

Figure 6. Short-time-averaged distances $\langle r_i(t)\rangle_{sta}$ between each atom and the center of mass in Na_{142}, as functions of time at $T = 361$ K. The bold lines are to guide the eye in following the diffusive behavior of specific atoms.

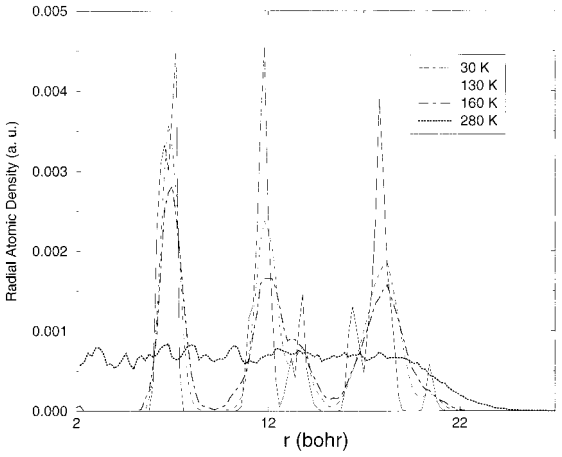

Figure 7. Time-averaged radial atomic densities of the icosahedral isomer of Na_{142} at some representative temperatures.

Figures 5 and 7 show that, at $T = 160$ K, the atomic shells of the Na_{142} cluster are still well-defined, but the movies reveal isomerization transitions, similar to those found at the begining of the melting-like transitions of Na_8 and Na_{20},[22] with no true diffusion. These isomerizations involve the motion of vacancies in the outer shell, in such a way that different isomers are visited while the icosahedral structure is preserved. The onset of this motion is gradual and does not lead to features in the specific heat, although it is detected in the temperature evolution of the diffusion coefficient (see Figure 8 and discussion below). The true surface melting stage does not develop in the icosahedral isomer until a temperature of $T_s \approx 240$ K is reached.

Figure 6 shows the time evolution of $\langle r_i\rangle_{sta}$ for Na_{142} at a temperature $T = 361$ K where the cluster is liquid with all of the atoms diffusing throughout the cluster. Some specific cases of atoms that are near (far from) the center of mass of the cluster at the begining of the simulation and end in a position far from (near) the center of mass of the cluster are shown in boldface. The atomic density distribution at 280 K, a temperature just above the melting point, is nearly uniform across the cluster, a radial expansion of the cluster by about 5 bohr units is evident, and the surface is more diffuse.

The $\langle r_i(t)\rangle_{sta}$ curves for Na_{92} at low temperature are qualitatively similar to those of Na_{142}. Na_{92} shows surface melting at

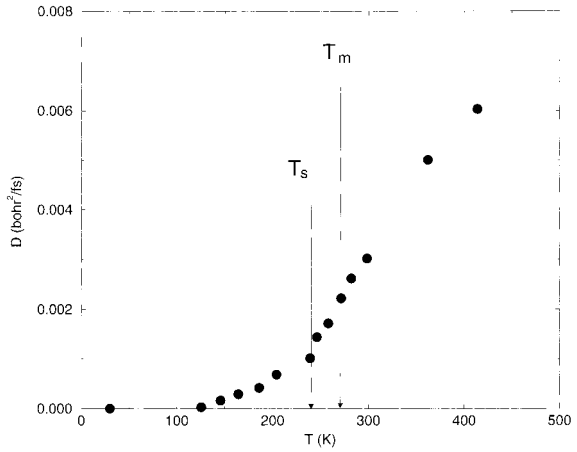

Figure 8. Diffusion coefficient as a function of temperature for the icosahedral isomer of Na_{142}.

$T_s \approx 130$ K. This temperature is in the range where the isomerization processes in Na_{142} set in, but the larger number of vacancies in the surface shell of Na_{92} allows for more rapid surface diffusion, which gives rise to a distinct peak in the specific heat.

Na_{55} is a perfect two-shell icosahedron, so surface atoms have no empty sites to which they can move, and diffusion within an atomic shell is almost as difficult as diffusion across different shells. When the surface atoms have enough energy to exchange positions with one another, they can just as easily migrate throughout the whole cluster, and melting proceeds in a single stage at 190 K. Calvo and Spiegelmann[9] have suggested that this one-step melting is associated with a large energy gap between the ground-state icosahedral structure and the closest low-lying isomers, but this cannot be a general result for perfect icosahedral metallic clusters, as the details of melting are material-dependent. For example, a surface melting stage has been observed in simulations of icosahedral Ni_{55}.[37]

The variation of the diffusion coefficient with temperature is shown in Figure 8 for Na_{142}. At temperatures less than about 140 K, D is close to zero, indicating only an oscillatory motion of the atoms. For temperatures between 140 K and T_s, the diffusion coefficient increases, indicating that the atoms in the cluster are not undergoing simple vibrational motion; the atomic motions are, nevertheless, of the special kind discussed above that preserve the icosahedral structure. The slope of $D(T)$ increases appreciably at T_s when surface melting occurs, but there is no noticeable feature when the cluster finally melts at T_m. The features of $D(T)$ for Na_{92}, which are not shown here, are very similar: $D(T)$ is very sensitive to the surface melting stage, where appreciable diffusive motion begins, and the homogeneous melting transition is masked by that effect. We conclude that the $D(T)$ curve is a good indicator of homogeneous melting only in those cases where the surface melting stage is absent, as, for example, in Na_{55}.

Our results suggest that the melting transition in large icosahedral sodium clusters occurs over a smaller temperature range than it does in small clusters such as Na_8 or Na_{20},[22] at least near an icosahedral-shell closing. Furthermore, the size of any prepeak diminishes with respect to the main homogeneous melting peak as the cluster size increases, that is, as the fraction of atoms that can take part in premelting decreases. Consequently, a homogeneous melting temperature can be defined with less ambiguity for large clusters. These comments apply to the caloric and specific heat curves, which are the quantities amenable to experimental measurement. In contrast,

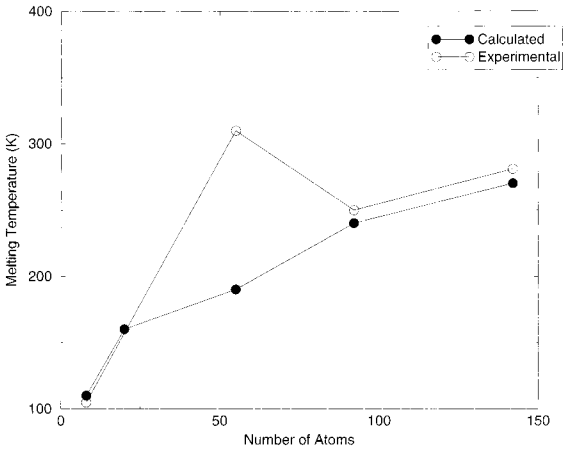

Figure 9. Calculated melting temperatures, compared with the experimental values. The experimental values for the larger cluster sizes are taken from ref 6, while that for the smallest Na_8 cluster is taken from ref 38 (see text for details).

microscopic quantities such as the diffusion coefficient D or the $\langle r_i(t)\rangle_{sta}$ curves are very sensitive to any small reorganization in the atomic arrangement, and it is difficult to determine the melting transition from the variation of these quantities with temperature. A helpful structural, as opposed to thermal, indicator of the melting transition in medium-sized or large clusters is the shape of the radial atomic density distribution. The atomic density displays a pronounced shell structure at low temperatures that is smoothed out at intermediate temperatures where the vacancy diffusion and/or surface melting mechanisms are present. Above T_m, the density is flat.

In Figure 9, we compare the calculated values of the melting temperature with the experimental values. Our earlier results for Na_8 and Na_{20}[22] are also included, although, for such small sizes, there is some ambiguity in defining a melting temperature. There is excellent agreement with the experimental results for Na_{92} and Na_{142}.[6] Measurements of the temperature dependence of the photoabsorption cross sections for Na_n^+ ($n = 4-16$) have recently been reported.[38,39] Although the spectra do not show evidence of a sharp melting transition, some encouraging comparisons between theory and experiment can be made. The experimental spectra do not change appreciably upon increasing the cluster temperature, until $T = 105$ K (the value given as the experimental melting temperature of Na_8 in Figure 9), where the spectra begin to evolve in a continuous way. In our study of the melting behavior of Na_8,[22] we found a broad transition starting at $T = 110$ K and continuing until $T = 220$ K, at which point the liquid state was fully developed. This might explain the absence of abrupt changes in the experimental photoabsorption spectrum with temperature. In any case, we feel that the good agreement between theory and experiment might extend to the small sizes. However, our method is not expected to yield accurate fine details in the melting temperature as a function of cluster size because of electronic-shell effects that are not accounted for in our approximate kinetic energy functional. The discrepancy for Na_{55} remains intriguing.

We finish this section with the observation that no dynamic coexistence or back bending of the caloric curves, phenomena that are intimately linked,[40] is detected in our microcanonical simulations. Nor do we observe any bimodal behavior in, say, the short-time average of the ionic kinetic energies. This might well be a consequence of the time scale of our simulations, which is significantly shorter than that of simulations using phenomenological potentials and which might be too short to allow observation of a single cluster fluctuating in time between solidlike and liquidlike phases. In any case, it could be difficult to observe the dynamic coexistence phenomenon in clusters as large as those studied here even with significantly longer simulation times. For example, Beck et al.[41] reported a slush behavior with no dynamical coexistence when the potential energy surface contained a large number of isomers separated by small energy barriers, which Kronik et al.[42] showed to be the case for sodium clusters. The importance of the dynamic coexistence phenomenon also decreases with increasing number of particles.[43] This is mainly due to entropic effects because it is very difficult for a large cluster in the liquid phase to find its way back to the solidlike catchment basin in the potential energy surface.

IV. Discussion and Conclusions

A few comments regarding the quality of the simulations are perhaps in order here. The orbital-free representation of the atomic interactions, although much more efficient than the more accurate KS treatments, is still substantially more expensive computationally than a simulation using phenomenological many-body potentials. Such potentials contain a number of parameters that are usually chosen by fitting some bulk and/or molecular properties. In contrast, our model is free of external parameters, although there are approximations in the kinetic and exchange-correlation functionals. The orbital-free scheme accounts, albeit approximately, for the effects of the detailed electronic distribution on the total energy and the forces on the ions. We feel that this is particularly important in metallic clusters for which a large proportion of atoms are on the surface and experience a very different electronic environment than atoms in the interior. Furthermore, the adjustment of the electronic structure, and consequently the energy and forces, to rearrangements of the ions is also taken into account. However, the price to be paid for the more accurate description of the interactions is a less complete statistical sampling of the phase space. The simulation times are substantially shorter than those that can be achieved in phenomenological simulations. Longer simulations would be needed to fully converge the heights of the specific heat peaks or to observe a van der Waals loop in the caloric curves, to mention two examples. Nevertheless, we expect that the locations of the various transitions are reliable. All of the indicators that we have used, both thermal and structural, are in essential agreement on the temperature at which the transitions start. As we discussed in a previous paper,[22] longer trajectories might induce just a slight lowering in the transition temperatures.

The melting-like transitions of Na_{142}, Na_{92}, and Na_{55} have been investigated by applying an orbital-free, density functional molecular dynamics method. The computational effort required is modest in comparison with that of the traditional Car−Parrinello molecular dynamics technique based on Kohn−Sham orbitals, which would be very costly for clusters of this size. Specifically, the computational effort to update the electronic system scales linearly with the system size N, in contrast to the N^3 scaling of orbital-based methods. This saving allows for the study of large clusters. However, the price to pay is an approximate electron kinetic energy.

An icosahedral isomer of Na_{142} melts in two steps, as evidenced by the thermal indicators. Nevertheless, there are isomerization transitions involving surface defects at temperatures as low as 130 K that preserve the icosahedral structure and do not give rise to any pronounced feature in the caloric curve. The transition at $T_s \approx 240$ K from the isomerization regime to a phase in which the surface atoms acquire a

substantial diffusive motion is best described as surface melting. This is followed at $T_m \approx 270$ K by homogeneous melting. For Na_{92}, there is a minor peak in C_v at $T_s \approx 130$ K that we associate with surface melting. The smaller value of T_s, for this cluster compared with Na_{142}, is due to the less-ordered surface. Na_{55}, being a perfect two-shell icosahedron with no surface defects, melts in a single stage at 190 K. In all cases, for $T > T_m$, the atoms are able to diffuse throughout the cluster volume. Both the calculated T_m at which homogeneous melting occurs and the estimated latent heat of fusion q_m are in excellent agreement with the experimental results of Haberland and co-workers for Na_{142} and Na_{92}; our earlier results on the melting of Na_8[22] are also consistent with the variation in the measured optical spectrum with temperature. A serious discrepancy between theory and experiment remains for Na_{55}.

We have found that structural quantities obtained from simulations that are very useful in the study of melting in small clusters,[22] such as the diffusion coefficient, are not, in the case of the larger clusters studied here, efficient indicators of homogeneous melting, which is better located with thermal indicators. A better structural indicator is the evolution with temperature of the average radial ion density. This quantity flattens when homogeneous melting occurs.

Acknowledgment. We thank H. Haberland, S. Kümmel, and F. Calvo for sending us preprints of their respective works prior to publication and María J. López for useful discussions. This work has been supported by DGES (Grants PB95-0720-C02-01, PB98-0345, and PB98-0368) and Junta de Castilla y Léon (VA28/99 and VA70/99). A. Aguado acknowledges a graduate fellowship from Junta de Castilla y Léon. M. J. Stott acknowledges the support of the NSERC of Canada and an Iberdrola Visiting Professorship at the University of Valladolid.

References and Notes

(1) Ellert, C.; Schmidt, M.; Schmitt, C.; Reiners, T.; Haberland, H. *Phys. Rev. Lett*. **1995**, *75*, 1731. Brockhaus, P.; Wong, K.; Hansen, K.; Kasperovich, V.; Tikhonov, G.; Kresin, V. *Phys. Rev. A* **1999**, *59*, 495.

(2) Wang, Z. L.; Petroski, J. M.; Green, T. C.; El-Sayed, M. A. *J. Phys. Chem. B* **1998**, *102*, 6145.

(3) Martin, T. P. *Phys. Rep*. **1996**, *273*, 199.

(4) Peters, K. F.; Cohen, J. B.; Chung, Y. W. *Phys. Rev. B* **1998**, *57*, 13430.

(5) Maier-Borst, M.; Cameron, D. B.; Rokni, M.; Parks, J. H. *Phys. Rev. A* **1999**, *59*, R3162.

(6) Schmidt, M.; Kusche, R.; Kronmüller, W.; von Issendorff, B.; Haberland, H. *Phys. Rev. Lett*. **1997**, *79*, 99. Schmidt, M.; Kusche, R.; von Issendorff, B.; Haberland, H. *Nature* **1998**, *393*, 238. Kusche, R.; Hippler, T.; Schmidt, M.; von Issendorff, B.; Haberland, H. *Eur. Phys. J. D* **1999**, *9*, 1.

(7) Jellinek, J.; Beck, T. L.; Berry, R. S. *J. Chem. Phys*. **1986**, *84*, 2783. Davis, H. L.; Jellinek, J.; Berry, R. S. *J. Chem. Phys*. **1987**, *86*, 6456. Rose, J. P.; Berry, R. S. *J. Chem. Phys*. **1992**, *96*, 517; **1993**, *98*, 3262. Cheng, V. K. W.; Rose, J. P.; Berry, R. S. *Surf. Rev. Lett*. **1996**, *3*, 347. Calvo, F.; Labastie, P. *J. Phys. Chem. B* **1998**, *102*, 2051. Doye, J. P. K.; Wales, D. *J. Phys. Rev. B* **1999**, *59*, 2292; *J. Chem. Phys*. **1999**, *111*, 11070. Bulgac, A.; Kusnezov, D. *Phys. Rev. Lett*. **1992**, *68*, 1335; *Phys. Rev. B* **1992**, *45*, 1988. Ju, N.; Bulgac, A. *Phys. Rev. B* **1993**, *48*, 2721. Fosmire, M.; Bulgac, A. *Phys. Rev. B* **1995**, *52*, 17509; *Z. Phys. D* **1999**, *40*, 458. Bulgac, A. *Z. Phys. D* **1997**, *40*, 454. Thompson, J. M.; Bulgac, A. *Z. Phys. D* **1997**, *40*, 462. Rey, C.; Gallego, L. J.; García-Rodeja, J.; Alonso, J. A.; Iñiguez, M. P. *Phys. Rev. B* **1993**, *48*, 8253. García-Rodeja, J.; Rey, C.; Gallego, L. J.; Alonso, J. A. *Phys. Rev. B* **1994**, *49*, 8496. Lewis, L. J.; Jensen, P.; Barrat, J. L. *Phys. Rev. B* **1997**, *56*, 2248. Nayak, S. K.; Khanna, S. N.; Rao, B. K.; Jena, P. *J. Phys: Condens. Matter* **1998**, *10*, 10853.

(8) Cleveland, C. L.; Luedtke, W. D.; Landman, U. *Phys. Rev. Lett*. **1998**, *81*, 2036; *Phys. Rev. B* **1999**, *60*, 5065.

(9) Calvo, F.; Spiegelmann, F. *Phys. Rev. Lett*. **1999**, *82*, 2270; *J. Chem. Phys*. **2000**, *112*, 2888.

(10) Yurtsever, E.; Calvo, F. *Phys. Rev. B* **2000**, *62*, 9977.

(11) Car, R.; Parrinello, M. *Phys. Rev. Lett*. **1985**, *55*, 2471. Payne, M. C.; Teter, M. P.; Allan, D. C.; Arias, T. A.; Joannopoulos, J. D. *Rev. Mod. Phys*. **1992**, *64*, 1045.

(12) Röthlisberger, U.; Andreoni, W. *J. Chem. Phys*. **1991**, *94*, 8129.

(13) Rytkönen, A.; Häkkinen, H.; Manninen, M. *Phys. Rev. Lett*. **1998**, *80*, 3940.

(14) Kohn, W.; Sham, L. J. *Phys. Rev*. **1965**, *140*, 1133A.

(15) Hohenberg, P.; Kohn, W. *Phys. Rev*. **1964**, *136*, 864B.

(16) Chaćon, E.; Alvarellos, J. E.; Tarazona, P. *Phys. Rev. B* **1985**, *32*, 7868. García-González, P.; Alvarellos, J. E.; Chacón, E. *Phys. Rev. B* **1996**, *53*, 9509; *Phys. Rev. A* **1996**, *54*, 1897; *Phys. Rev. B* **1998**, *57*, 4857; *Phys. Rev. A* **1998**, *57*, 4192.

(17) Pearson, M.; Smargiassi, E.; Madden, P. A. J. *Phys.: Condens. Matter* **1993**, *5*, 3221. Smargiassi, E.; Madden, P. A. *Phys. Rev. B* **1994**, *49*, 5220. Foley, M.; Smargiassi, E.; Madden, P. A. *J. Phys.: Condens. Matter* **1994**, *6*, 5231. Smargiassi, E.; Madden, P. A. *Phys. Rev. B* **1995**, *51*, 117; **1995**, *51*, 129. Foley, M.; Madden, P. A. *Phys. Rev. B* **1996**, *53*, 10589. Jesson, B. J.; Foley, M.; Madden, P. A. *Phys. Rev. B* **1997**, *55*, 4941. Anta, J. A.; Jesson, B. J.; Madden, P. A. *Phys. Rev. B* **1998**, *58*, 6124.

(18) Govind, N.; Wang, Y. A.; Carter, E. A. *J. Chem. Phys*. **1999**, *110*, 7677. Wang, Y. A.; Govind, N.; Carter, E. A. *Phys. Rev. B* **1999**, *60*, 16350. Watson, S. C.; Carter, E. A. *Comput. Phys. Commun*. **2000**, *128*, 67.

(19) Shah, V.; Nehete, D.; Kanhere, D. G. *J. Phys.: Condens. Matter* **1994**, *6*, 10773. Nehete, D.; Shah, V.; Kanhere, D. G. *Phys. Rev. B* **1996**, *53*, 2126. Shah, V.; Kanhere, D. G. *J. Phys.: Condens. Matter* **1996**, *8*, L253. Shah, V.; Kanhere, D. G.; Majumber, C.; Das, G. P. *J. Phys.: Condens. Matter* **1997**, *9*, 2165. Vichare, A.; Kanhere, D. G. *J. Phys.: Condens. Matter* **1998** *10*, 3309; *Eur. Phys. J. D* **1998**, *4*, 89. Dhavale, A.; Shah, V.; Kanhere, D. G. *Phys. Rev. A* **1998** *57*, 4522

(20) Govind, N.; Mozos, J. L.; Guo, H. *Phys. Rev. B* **1995**, *51*, 7101. Wang, Y. A.; Govind, N.; Carter, E. A. *Phys. Rev. B* **1998**, *58*, 13465.

(21) Blaise, P.; Blundell, S. A.; Guet, C. *Phys. Rev. B* **1997**, *55*, 15856.

(22) Aguado, A.; Lopez, J. M.; Alonso, J. A.; Stott, M. J. *J. Chem. Phys*. **1999**, *111*, 6026.

(23) *Theory of the Inhomogeneous Electron Gas*; Lundqvist, S., March, N. H., Eds.; Plenum Press: New York, 1983.

(24) Yang, W. *Phys. Rev. A* **1986**, *34*, 4575.

(25) Perdew, J. P. *Phys. Lett. A* **1992**, *165*, 79.

(26) Perdew, J. P.; Zunger, A. *Phys. Rev. B* **1981**, *23*, 5048.

(27) Ceperley, D.; Alder, B. *Phys. Rev. Lett*. **1980**, *45*, 566.

(28) Fiolhais, C.; Perdew, J. P.; Armster, S. Q.; McLaren, J. M.; Brajczewska, H. *Phys. Rev. B* **1995**, *51*, 14001; **1996**, *53*, 13193.

(29) Nogueira, F.; Fiolhais, C.; He, J.; Perdew, J. P.; Rubio, A. *J. Phys.: Condens. Matter* **1996**, *8*, 287.

(30) Verlet, L. *Phys. Rev*. **1967**, *159*, 98. Swope, W. C.; Andersen, H. C. *J. Chem. Phys*. **1982**, *76*, 637.

(31) Montejano-Carrizales, J. M.; Iñiguez, M. P.; Alonso, J. A.; López, M. *J. Phys. Rev. B* **1996**, *54*, 5961.

(32) Sugano, S. *Microcluster Physics*; Springer-Verlag: Berlin, 1991.

(33) Pearson, E. M.; Halicioglu, T.; Tiller, W. A. *Phys. Rev. A* **1985**, *32*, 3030.

(34) Kümmel, S.; Reinhard, P. G.; Brack, M. *Eur. Phys. J. D* **1999**, *9*, 149. Kümmel, S.; Brack, M.; Reinhard, P. G. *Phys. Rev. B* **2000**, *62*, 7602.

(35) Montag, B.; Reinhard, P. G. *Z. Phys. D* **1995**, *33*, 265.

(36) Martin, T. P.; Bergmann, T.; Göhlich, H.; Lange, T. *Z. Phys. D* **1991**, *19*, 25.

(37) Güvenc, Z. B.; Jellinek, J. *Z. Phys. D* **1993**, *26*, 304.

(38) Schmidt, M.; Ellert, C.; Kronmüller, W.; Haberland, H. *Phys. Rev. B* **1999**, *59*, 10970.

(39) Haberland, H. *Metal Clusters*; Ekardt, W., Ed.; John Wiley & Sons: New York, 1999; p 181.

(40) Wales, D. J.; Berry, R. S. *Phys. Rev. Lett*. **1994**, *73*, 2875.

(41) Beck, T. L.; Jellinek, J.; Berry, R. S. *J. Chem. Phys*. **1987**, *87*, 545.

(42) Kronik, L.; Vasiliev, I.; Chelikowsky, J. R. *Phys. Rev. B* **2000**, *62*, 9992.

(43) Rose, J. P.; Berry, R. S. *J. Chem. Phys*. **1993**, *98*, 3246.